A COMPACT OPTICAL ATOMIC CLOCK BASED ON A TWO-PHOTON TRANSITION IN RUBIDIUM

Kyle W. Martin, et al.

29 May 2019

Interim Report

AIR FORCE RESEARCH LABORATORY
Space Vehicles Directorate
3550 Aberdeen Ave SE
AIR FORCE MATERIEL COMMAND
KIRTLAND AIR FORCE BASE, NM 87117-5776

REPORT DOCUMENTATION PAGE

Form Approved
OMB No. 0704-0188

1. REPORT DATE *(DD-MM-YYYY)* 29-05-2019	2. REPORT TYPE Interim Report	3. DATES COVERED *(From - To)* 18 Aug 2015 – 08 Aug 2017

4. TITLE AND SUBTITLE	5a. CONTRACT NUMBER

A Compact Optical Atomic Clock Based on a Two-Photon Transition in Rubidium

5b. GRANT NUMBER

5c. PROGRAM ELEMENT NUMBER
62601F

6. AUTHOR(S)
Kyle W. Martin[1], Gretchen Phelps, Nathan D. Lemke, Matthew S. Bigelow[1], Benjamin Stuhl[2], Michael Wojcik[2], Michael Holt[2], Ian Coddington[3], Michael W. Bishop, and John H. Burke

5d. PROJECT NUMBER
1010

5e. TASK NUMBER
PPM00015883

5f. WORK UNIT NUMBER
EF121263

7. PERFORMING ORGANIZATION NAME(S) AND ADDRESS(ES)
Air Force Research Laboratory, Space Vehicles Directorate, 3550 Aberdeen Avenue SE, Kirtland AFB, NM 87117-5776
[1]Applied Technology Associates dba ATA, 1300 Britt Street SE, Albuquerque, NM 87123
[2]Space Dynamics Laboratory, 1695 North Research Park Way, North Logan, UT 84341
[3]National Institute of Standards and Technology, 325 Broadway, Boulder, CO 80305

8. PERFORMING ORGANIZATION REPORT NUMBER
AFRL-RV-PS-TR-2019-0065

9. SPONSORING / MONITORING AGENCY NAME(S) AND ADDRESS(ES)

10. SPONSOR/MONITOR'S ACRONYM(S)
AFRL/RVBN

11. SPONSOR/MONITOR'S REPORT NUMBER(S)

12. DISTRIBUTION / AVAILABILITY STATEMENT
Approved for public release; distribution is unlimited. (377ABW-2017-14825 dtd 13 Sep 2017)

13. SUPPLEMENTARY NOTES

14. ABSTRACT
We describe a vapor cell-based optical atomic clock that utilizes the 778 nm two-photon transition in rubidium and yields fractional frequency instabilities of $3\times10^{-13}/\sqrt{\tau(s)}$ for τ from 1 s to 10000 s. We present a complete stability budget and describe the required conditions under which the system could maintain a fractional frequency instability of 1×10^{-15} on long timescales. The system is constructed primarily from commercially-available components, an attractive feature from the standpoint of commercialization and deployment of optical frequency standards.

15. SUBJECT TERMS
optical atomic clock, rubidium frequency standard, two-photon transition

16. SECURITY CLASSIFICATION OF:			17. LIMITATION OF ABSTRACT	18. NUMBER OF PAGES	19a. NAME OF RESPONSIBLE PERSON Dr. Gretchen Phelps
a. REPORT Unclassified	b. ABSTRACT Unclassified	c. THIS PAGE Unclassified	Unlimited	12	19b. TELEPHONE NUMBER *(include area code)*

Standard Form 298 (Rev. 8-98)
Prescribed by ANSI Std. 239.18

A Compact Optical Atomic Clock Based on a Two-Photon Transition in Rubidium[*]

Kyle W. Martin,[1] Gretchen Phelps,[2] Nathan D. Lemke,[2] Matthew S. Bigelow,[1] Benjamin Stuhl,[3]
Michael Wojcik,[3] Michael Holt,[3] Ian Coddington,[4] Michael W. Bishop,[2] and John H. Burke[2]

[1] *Applied Technology Associates dba ATA, 1300 Britt Street SE Albuquerque, NM 87123*
[2] *Air Force Research Laboratory, Space Vehicles Directorate Kirtland Air Force Base 87117*
[3] *Space Dynamics Laboratory, 1695 North Research Park Way North Logan, Utah 84341*
[4] *National Institute of Standards and Technology, 325 Broadway Boulder, CO 80305*
(Dated: August 18, 2017)

We describe a vapor cell-based optical atomic clock that utilizes the 778 nm two-photon transition in rubidium and yields fractional frequency instabilities of $3 \times 10^{-13}/\sqrt{\tau(s)}$ for τ from 1 s to 10000 s. We present a complete stability budget and describe the required conditions under which the system could maintain a fractional frequency instability of 1×10^{-15} on long timescales. The system is constructed primarily from commercially-available components, an attractive feature from the standpoint of commercialization and deployment of optical frequency standards.

I. INTRODUCTION

High stability clocks and oscillators play an integral role in many modern technologies such as navigation and communications [1]. Laboratory-based primary frequency standards, which utilize RF transitions between atomic hyperfine levels, provide the highest degree of timing accuracy and are used to form international timescales [2, 3]; in many cases, however, applications beyond timekeeping require clocks that are deployed outside the laboratory setting. One well-known case is that of global navigation satellite systems (GNSS), which employ space-qualified frequency standards aboard satellites in medium earth orbit and/or geosynchronous orbit [1, 4]. While portable clocks are typically outpaced by their laboratory counterparts in terms of precision and accuracy, they nonetheless offer very low frequency instabilities; in the case of rubidium atomic frequency standards, clocks are commercially available with a drift rate below 10^{-13}/day and a frequency noise floor less than 10^{-14} [5].

With the advent of fully stabilized optical frequency combs in 2000 [6–8], optical frequency standards have rapidly surpassed the capabilities of RF clocks in both stability [9, 10] and systematic uncertainty [11–13]. However, these improvements have yet to make an impact on portable and deployable clocks. Much of the difficulty in developing compact and environmentally robust optical frequency standards lies with the complicated laser sources and optical systems required for laser cooling and interrogating an atomic sample. Moreover, given the high quality factor (i.e. narrow spectral linewidth) of typical optical clock transitions, laser pre-stabilization to a high-finesse Fabry-Pérot cavity is generally required, which adds significant complexity to the system. Finally, optical frequency combs have historically not been sufficiently compact or robust to warrant an effort toward deployment.

With these challenges in mind, we investigate an optical clock based on a two-photon transition in a hot Rb vapor. Two-photon transitions are attractive because they enable Doppler-free spectra [14] without the need for laser-cooling, provided two anti-parallel laser beams are used to interrogate the atomic vapor. Moreover, the two-photon transition can often be observed via a fluorescence signal that is spectrally resolvable from the probe laser; together with the large number of atoms interrogated in the vapor phase, this enables a very high signal-to-noise measurement of the clock transition probability. For the case of the Rb two-photon transition at 778 nm, fluorescence is readily observable at 420 nm, and stray light in the near infrared is rejected with standard optical filtering. We further benefit in the case of the Rb $5S_{1/2} \rightarrow 5D_{5/2}$ transition from the nearby intermediate state $5P_{3/2}$ that is only 2 nm detuned from the virtual two-photon state (see Figure 1), facilitating significant atomic excitation rates at modest optical intensities [15–17]. Conveniently, 778.1 nm light can be produced by second harmonic generation (SHG) of 1556.2 nm, which falls in the telecommunications C-band, allowing the use of mature laser sources and erbium fiber frequency combs [18–20]. Of particular benefit is the availability of commercial laser systems for which the fast linewidth is significantly below the natural linewidth of the excited clock state ($\Delta\nu \approx 330$ kHz as observed at 778 nm), alleviating the requirement for laser pre-stabilization to a high finesse optical cavity.

These appealing features motivate our investigation of an optical Rb atomic frequency standard ("O-RAFS") as a future portable clock. While our work has not yet specifically designed the system for a small footprint and low power consumption, we anticipate this should be possible. As a first step, however, it must be shown that a vapor cell-based two-photon clock can meet the demanding timing requirements needed to enable the above applications. Of particular interest is a frequency standard that can surpass existing RF clocks by one factor of 10 in both short- and long-term stabilities, which would translate to an Allan deviation of $\sim 1 \times 10^{-13}$ at 1 s and $\sim 1 \times 10^{-15}$ at

---

1

1 day. Previous investigations into this transition in Rb were carried out in the 1990s [15–17] with some renewed interest recently leveraging the development of laser and frequency comb technologies [21–23]. While initial experiments showed the system to be capable of instabilities as low as $3 \times 10^{-13}/\sqrt{\tau}$ for τ from 1–2000 s, on longer timescales the instability increased [17], and instability below 1×10^{-14} has not been observed. Here, we extend the range of integration to longer timescales and demonstrate a corresponding reduction of long-term instability, approaching the level of 1×10^{-15}. Key to this level of performance are tight control over the vapor density [24] and laser power [17], both of which we describe in detail below, together with a full stability budget for the frequency standard.

This paper is organized as follows. Section II describes the design of the frequency standard and measurement system. Section III provides detailed analysis of the known contributors to clock instability, with particular emphasis on the clock laser-induced AC Stark shift, collisional effects, and Zeeman shifts. The performance of the frequency standard is detailed in Section IV, and the paper concludes with a discussion of conceived upgrades to the two-photon frequency standard in Section V.

II. EXPERIMENTAL APPARATUS

The design shown in Figure 2 begins with a 1556 nm diode laser system that produces 20 mW of narrow-band light (fast linewidth $\leq$ 2 kHz.) This laser acts as the local oscillator for the frequency standard. A small portion of the seed laser output is sampled by a fiber splitter to form an optical beat note with a fiber frequency comb based upon the design in [20]; the frequency comb coherently divides the 385 THz optical waveform to $\sim$ 160 MHz, which is the comb's pulse repetition rate. After stabilization of the optical beatnote and carrier envelope offset frequency, the comb's repetition rate is photodetected and compared to a hydrogen maser via a phase noise measurement device. The remaining portion of the 1556 nm laser output enters a fiber-coupled electro-optic modulator (EOM) formed in a proton-exchange waveguide embedded in lithium niobate, which is driven at 130 kHz. After the EOM, the light is amplified by an erbium-doped fiber amplifier and undergoes second harmonic generation (SHG) in a periodically poled lithium niobate (PPLN) crystal. The output of the SHG crystal is subsequently sent through a variable optical attenuator (VOA), which is used for laser power stabilization as described below. Typically 30 mW of 778 nm light is then delivered to the vapor cell assembly.

The vapor cell assembly is enclosed in a 5 mm-thick, single layer mu-metal magnetic shield, to reduce spectral broadening associated with the Zeeman shift. The vapor cell is heated to 100 °C to generate sufficient vapor density for a high stability clock. To avoid local magnetic fields when heating the vapor cell, all heat is generated
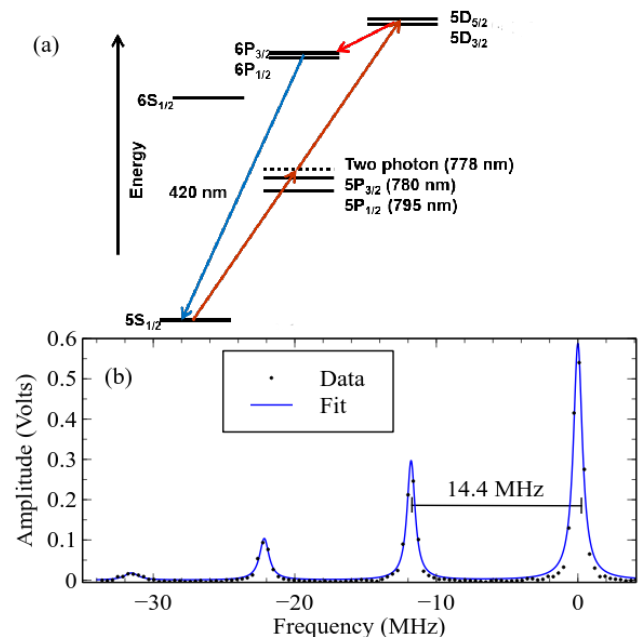

FIG. 1. (a) Partial energy level diagram of Rb. The virtual state associated with two-photon excitation at 778 nm is shown by the dashed line. The cascade decay path $5D_{5/2} \rightarrow 6P_{3/2} \rightarrow 5S_{1/2}$ results in the emission of a 420 nm photon, which we use to observe the two-photon resonance. (b) Two-photon excitation spectrum of ^{87}Rb (F=2). The frequency axis is presented as the 778 nm laser detuning from the F=2→F'=4 transition, which has the largest Clebsch-Gordan coefficient. Included is a fit using a sum of four Lorentzian peaks of equal width and with relative peak heights and detunings constrained by the values presented in [15]. The fitting procedure results in a full-width at half-maximum linewidth of 609 kHz, which exceeds the natural linewidth by a factor of 1.8, which we expect is due to line broadening from helium collisions [24].

with resistive and thermo-electric devices located outside the magnetic shielding; water-filled heat pipes protrude through the magnetic shield and provide heat to the dual-zone temperature control stage surrounding the vapor cell. The vapor cell, containing $>$ 99% isotopically enriched ^{87}Rb, is placed such that it has a 1 K thermal gradient along its length, forcing the cell's cold spot on the pinched-off fill tube of the borosilicate glass cell.

The 778 nm laser output is delivered by polarization-maintaining optical fiber through an opening in the magnetic shield, where it is collimated ($1/e^2$ intensity radius $w_0 = 0.66$ mm) using a non-magnetic optical assembly. A calcite Glan-Taylor polarizer is placed at the output of the fiber launcher to reduce polarization wander. The laser beam is sampled by a glass plate pick-off for laser power monitoring and sent through the vapor cell at Brewster's angle. A cat's eye retro-reflector [25] provides a precisely anti-parallel reflected beam, which is necessary for eliminating Doppler broadening. A portion of the fluorescence at 420 nm passes through a short-pass optical filter and is detected by photomultiplier tube
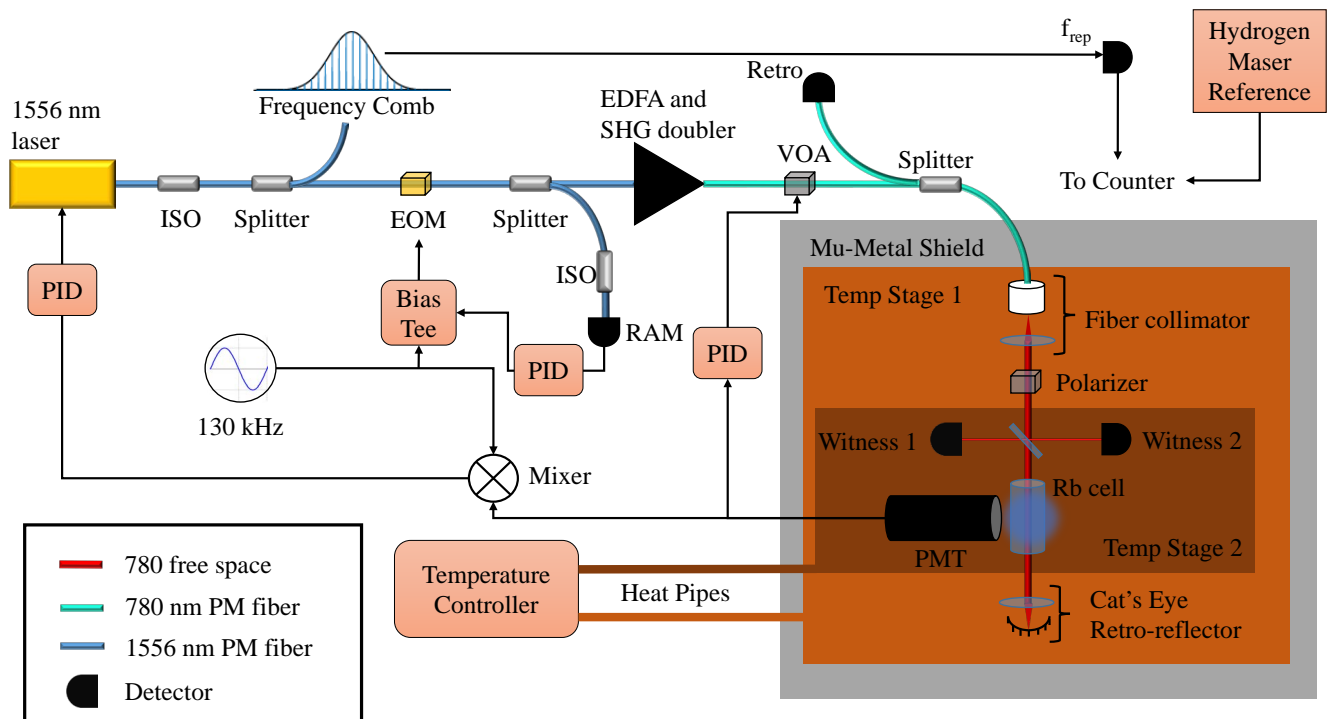
FIG. 2. An optical and simplified electrical schematic of the Rb two-photon frequency standard as described in the text. EOM - electro-optic modulator; PMT - photomultiplier tube; VOA - variable optical attenuator; ISO - optical isolator; EDFA - erbium doped fiber amplifier; SHG - second harmonic generator; RAM - residual amplitude modulation; PID - proportional integral differential lock mechanism.

(PMT). The PMT provides a fast temporal response and high electron-multiplying gain. After a transimpedance amplifier, the PMT output signal is demodulated by the 130 kHz sinusoidal modulation applied to the EOM in a phase detector, resulting in a laser detuning-dependent error signal. A digital servo controller with dual integrators feeds the 1556 nm laser's current to hold the laser on the two-photon resonance.

This design allows for the study of various parameters that contribute to the system's performance at different time scales. The short-term stability is determined by the atomic linewidth, optical intensity, detector collection efficiency, and laser frequency noise characteristics. The long-term stability, with a current goal of $< 1 \times 10^{-15}$ at one day, requires the stabilization of various experimental and environmental parameters including the vapor cell temperature (Rb vapor density), magnetic field, and optical power; these parameters are investigated in subsequent sections.

III. SOURCES OF CLOCK INSTABILITY

In this section we discuss the leading sources of instability to the Rb two-photon system. Particular importance is paid to rigorously determining the relevant sensitivity coefficients. Because our goals call for a sta-

ble frequency standard but not necessarily one with high accuracy, we do not undertake to precisely measure the magnitude of systematic effect, but rather to characterize the stability requirements of external parameters such as magnetic field and laser power. Table I summarizes all of the clock shifts and environmental stability parameters necessary to achieve fractional frequency instabilities of 1×10^{-15}.

A. AC Stark shift

Two-photon transitions are well-known to suffer from sizable AC Stark shifts associated with the probe laser [14]. The fractional AC Stark shift is given by

$$\frac{\Delta\nu}{\nu_0} = \frac{\Delta\alpha}{2c\epsilon_0 h}\overline{I(r)} = k(w_0)P, \qquad (1)$$

where $\overline{I(r)} \propto P/w_0^2$ is the spatially-averaged laser intensity, P is the one-way optical power incident on the vapor, $\nu_0 \approx 385$ THz is the two-photon laser frequency, and $\Delta\alpha$ is the differential polarizability of the two clock states at 778.1 nm. We measured the shift experimentally utilizing the clock laser detailed in Figure 2 together with an external Ti:sapphire laser. The Ti:sapphire laser
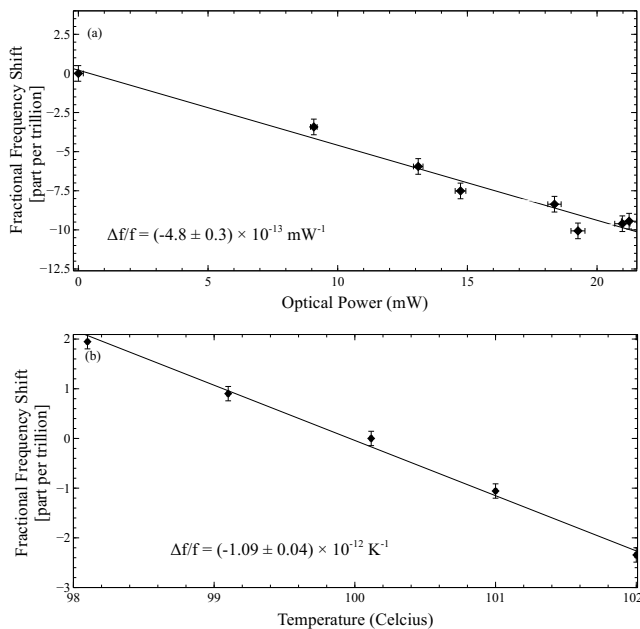
FIG. 3. (a) Experimentally measured 778 nm AC Stark shift for a (0.66 ± 0.05) mm beam. The fit used was orthogonal distance regression (ODR) which weights error bars in x and y data yielding a reduced χ^2 of 1.57 (b) Experimentally measured Rb collisional shifts, fit with ODR yielding a reduced χ^2 of 0.908.

FIG. 4. Magnetic field splitting for the $5D_{5/2}$ states of ^{87}Rb.

was tuned slightly away from the two-photon resonance by 2.6 GHz to an optical frequency of 385287.8 GHz, far enough detuned to induce no measurable excitation of the vapor, yet near enough to not significantly change the atomic polarizability. The two lasers were combined by a 50:50 beamsplitter and coupled into a single mode fiber, thereby enforcing the same spatial mode. Without changing the florescence signal size, which would contaminate the Stark shift measurement via lock point fluctuations, we varied the power of the detuned laser and measured the associated shift.

The results of this measurement are shown in Figure 3 along with a linear regression used to determine the sensitivity coefficient $k(w_0)$. The measured fractional clock shift coefficient is $4.8(4) \times 10^{-13}$/mW for $w_0 = 0.66(5)\mu$m. A previous measurement [17], appropriately scaled to match our beam radius, reports a coefficient of $4.5(4) \times 10^{-13}$/mW, which agrees well within the error bars of the two measurements. This coefficient indicates that the optical power must be stabilized to 2.1 μW to achieve 1×10^{-15} clock instability, requiring a precise laser power controller. A laser power stabilization circuit was constructed (Figure 2) using feedback to a fiber-optic variable optical attenuator. We found it most effective to use the fluorescence signal detected on the photomultiplier tube as the laser power sensor, rather than a sampled beam measured on a photodiode, although the latter is used as an out-of-loop witness sen-
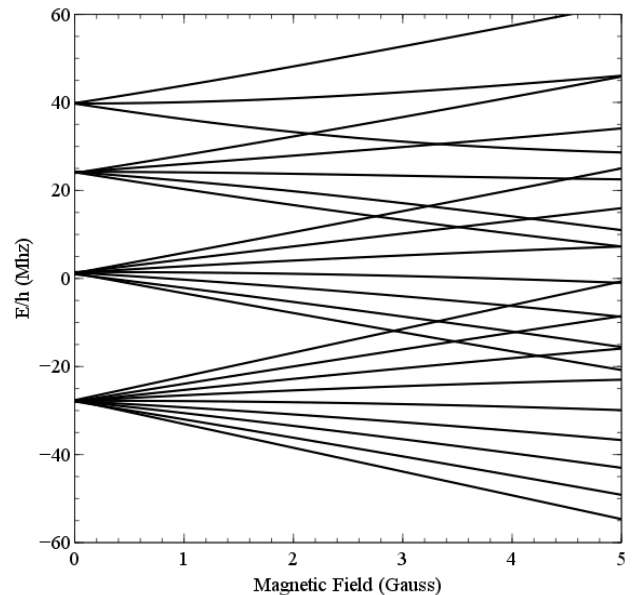
sor. This out-of-loop data was used to determine the fractional clock limitation imposed by laser power instability as shown in Figure 5.

B.   Zeeman shift

Stray magnetic fields are an important environmental variable that can produce substantial atomic frequency shifts. The magnetic field shift in the incomplete Paschen-Bach regime of the $5S_{1/2}$ ground state can be analytically calculated utilizing the Briet-Rabi formula; because our spectroscopic technique does not resolve transitions between specific magnetic sublevels, we then average over all relevant m_I and m_J magnetic quantum numbers. This assumption results in no first-order (linear) dependence of the clock frequency on magnetic field, and is valid for local magnetic fields $\lesssim 100$ mG, which is roughly the field at which Zeeman-induced line-broadening exceeds the natural linewidth of the two-photon transition. Substitution of the Landé g-factors and the magnetic dipole constant from Refs. [26, 27] yields a second order state shift of 114 Hz/G^2 for ^{87}Rb (F=2) and 358 Hz/G^2 for ^{85}Rb (F=3). The clock shift for the $5D_{5/2}$ excited state does not have an analytical

solution. The Hamiltonian,

$$\boldsymbol{H} = \boldsymbol{H}_{hfs} + \boldsymbol{H}_B^{(hfs)},$$

$$\boldsymbol{H}_{hfs} = A_{hfs}\frac{\boldsymbol{I}\cdot\boldsymbol{J}}{\hbar^2}$$

$$+ B_{hfs}\frac{\frac{3}{\hbar^2}(\boldsymbol{I}\cdot\boldsymbol{J})^2 + \frac{3}{2\hbar}(\boldsymbol{I}\cdot\boldsymbol{J}) - J(J+1)I(I+1)}{2I(2I-1)J(2J-1)},$$

$$\boldsymbol{H}_B^{(hfs)} = \mu_B(g_J\boldsymbol{J_z} + g_I\boldsymbol{I_Z})B,$$

was generated and diagonalized numerically. Substituting the magnetic dipole and quadrupole constants, A_{hfs} and B_{hfs}, for the $5D_{5/2}$ level from Ref. [15] results in a state shift of 50 kHz/G^2 for ^{87}Rb (F=4) and 190 kHz/G^2 for ^{85}Rb (F=5). The net clock shift is 6.5×10^{-11}/G^2 for ^{87}Rb and 2.5×10^{-10}/G^2 for ^{85}Rb. The energy level splitting diagram for the exited state of ^{87}Rb is shown in Figure 4. With these coefficients, we can now specify the magnetic shielding requirements; for ^{87}Rb (^{85}Rb), the magnetic field should be stable at the 3.9 mG (2.0 mG) level We installed a rectangular μ-metal shield of thickness 5 mm for which the expected shielding factor exceeds 1000. In practice, the shielding factor is reduced to due to openings for the heat pipes, optical fiber, electrical cabling, and photomultiplier tube, but we nonetheless expect the residual magnetic field at the vapor cell to be $\lesssim 1$ mG.

C. Collisional shift

The vapor cell temperature was determined using a standard 100 ohm resistive temperature detector (RTD) four wire measurement, with a duplicate device for out-of-loop monitoring. Two independent temperature control stages were designed, a 333 K plate (temperature stage 1 in Figure 2), to provide a stable reference temperature for heat transfer control, and a second, more finely controlled 373 K stage (temperature stage 2) upon which the vapor cell was mounted (see Figure 2). These stages were separated by four G-11 fiberglass posts to provide conductive thermal isolation. A precision temperature controller regulated a thermoelectric device and closed the temperature servo loops. Fiberglass insulation was added around the temperature control stages to reduce convective heat loss.

We measured a collisional shift for our ^{87}Rb enriched vapor cell by varying the vapor cell temperature. For each temperature change the system was allowed to thermalize, whereupon the resulting frequency shift was measured over 300 s.

The obtained frequency vs. temperature is plotted in Figure 3, and the fit supports a clock shift of $-1.09(4) \times 10^{-12}$/K, which is a factor of 2 larger than reported for natural ^{85}Rb by Zameroski et al. [24] . At 373 K the temperature must be stable to 0.92 mK to achieve fractional frequency stability of 1×10^{-15}. The fractional clock limitation caused by the temperature fluctuations of temperature stage 2, measured by the out-of-loop RTD, is shown in Figure 5.

D. Other Considerations

A frequency modulation technique utilizing a phase modulator is employed to lock the laser to the Rb vapor. This technique is known to suffer from residual amplitude modulation (RAM) that arises when modulation sidebands are not equal in magnitude or opposite in phase [28, 29]. Zhang et al. developed a technique to suppress both in-phase and quadrature RAM [30] utilizing a feedback control of the phase modulator's DC bias and temperature, respectively. We employed a similar technique using a single feedback loop to the DC bias voltage, which was combined with a sinusoidal modulation signal on a bias tee as shown in Figure 2. This method yielded suppression of > 35 dB. Additionally, we find benefit in saturating the input to the 1556 nm optical amplifier, which provides a passive reduction of RAM of > 5 dB. While these two suppression mechanisms were sufficient to achieve fractional clock instabilities shown in Figure 5, further corrections to quadrature RAM could be implemented through stabilizing the temperature of the EOM to further decrease clock instabilities.

Doppler effects are largely eliminated by retroreflecting the laser beam that passes through vapor cell. However, residual broadening related to the absorption of two-photons from the same beam remains; this contribution to the lineshape is a Gaussian function with a full-width at half-maximum of $\sqrt{8k_BT\ln 2/mc^2}\nu_0 \approx$ 571 MHz for ^{87}Rb at $T =$373 K, k_B the Boltzmann constant, and m the atomic mass. Absorbing two photons from the same beam occurs with the same probability as absorbing one photon from each beam; however, the linewidth associated with the former process is 1000 times greater than the latter. Hence, the Doppler-broadened peak is not easily resolved, and residual Doppler effects are small.

The significant tails of the Lorentzian peaks of neighboring hyperfine transitions pull the spectral lines closer together, a phenomenon known as line-pulling. The amount by which a particular transition is shifted is calculated by summing over all relevant hyperfine Lorentzians with appropriate frequencies and strengths given by Ref. [15]. The two-photon transition is shifted by 0.477 Hz for ^{85}Rb and 0.030 Hz for ^{87}Rb.

Second-order Doppler broadening, taking into account first order relativistic corrections, is given by,

$$\frac{\delta\omega}{\omega} = \frac{\bar{v}^2}{2c^2}, \tag{2}$$

where $\bar{v}^2 = 8k_bT/m\pi$. For Rb at 373 K the fractional clock shift is 5×10^{-13} with a slope of 1×10^{-15}/K.

The atomic vapor is immersed in a bath of electromagnetic radiation whose spectrum follows Plank's Law. In many cases, the blackbody radiation (BBR) shift can be

TABLE I. The environmental variables that impact ^{87}Rb clock performance are listed along with the corresponding fractional frequency sensitivity coefficient. The right column tabulates the stability requirement for each parameter to support a fractional frequency instability of 1×10^{-15}.

Shift	Fractional Coefficient	Stability at one day
778 nm AC Stark	4.8×10^{-13}/mW	2.1 μW
Rb density	1.1×10^{-12}/K	0.92 mK
Blackbody Radiation	1.3×10^{-15}/K	770 mK
DC Stark	5.9×10^{-15}/(V/cm)^2	0.17 (V/cm)^2
2nd Order Doppler	1.0×10^{-15}/K	1.0 K
Zeeman	6.5×10^{-11}/G^2	3.9 mG
Helium Collisional	2.7×10^{-8}/Torr	3.6×10^{-8} Torr

FIG. 5. The fractional frequency instability plotted as a Total Modified Allan deviation for ^{87}Rb with $1/\sqrt{\tau}$ white noise (black) as well as anticipated limits on the clock stability arising from cell temperature fluctuations (blue) and laser power fluctuations (red).

treated as a DC Stark shift, since the radiation is far off resonance from all relevant atomic transitions [31]. However, the operational temperature of our system, 373 K, yields a blackbody spectrum that is nearly resonant with several transitions connecting to the $5D_{5/2}$ state. Farley and Wing derived this perturbation for hydrogen, helium and the alkali-metal atoms for electromagnetic radiation at 300 K [32]. Hilico *et al.* calculated, assuming a T^4 behavior, that the perturbation would yield a shift of –210 Hz with a local slope of ∼1 Hz/K [17] at 373 K. The fractional clock shift arising from BBR is 1.3×10^{-15}/K requiring that the blackbody source be held to temperatures more stable than 770 mK; however, atomic Rb transitions near resonance with the blackbody spectrum at 100 C possibly impact the accuracy of this estimate. The D.C. polarizability of the $5D_{5/2}$ state was measured in [33], and it exceeds that of the $5S_{1/2}$ state by a factor of ∼ 50 due to low-lying transitions to nearby levels. Using this polarizability, we calculate the fractional clock sensitivity to D.C. electric fields is 5.9×10^{-15}/(V/cm)^2. The magnetic shield surrounding the vapor cell assembly also acts as a Faraday cage to prevent external electric fields from reaching the atomic vapor. However, stray charge could accumulate on the glass vapor cell itself; any resulting patch potentials need to be stable at the 0.5 V level.

Experimentally determined collisional shifts in [24] for various noble gases were examined to put limits on vapor cell impurities. Helium is the only gas that is known to permeate our vapor cell with a shift rate of –2.1 MHz/Torr. Therefore, we obtain that a helium leak rate of $< 3.6 \times 10^{-8}$ Torr/day must be achieved in order to achieve fractional clock instabilities below 1×10^{-15}. The cell may also be permeable to methane, which has an atmospheric composition of about three times less than helium, but the shift rate due to methane has not been measured to our knowledge.
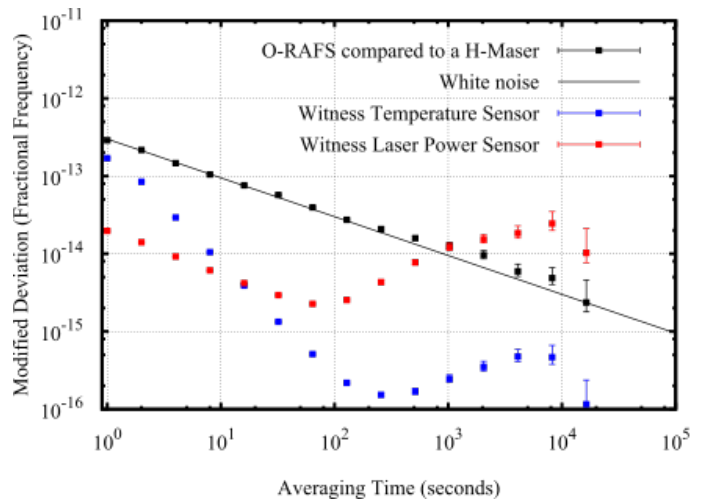
IV. RESULTS

Having assessed the leading contributions to instability, we next measured the clock performance by collecting the comb repetition rate on a phase noise measurement unit compared to a hydrogen maser. During data collection, the vapor cell temperature and 778 nm laser power were carefully monitored. The phase comparison was sampled at a rate of 1 Hz before being converted to frequency data, from which a linear drift of -8×10^{-19}/s was removed. Figure 5 shows the resulting total modified Allan deviation of the system, as well as the expected clock performance limitations derived from out-of-loop measurements of the cell temperature and laser power. Clock performance exceeds expected stability as calculated from laser power measurements, however, long term laser power measurements from the witness photodiode are thought to be partially influenced by room temperature fluctuations; leading to an overestimate of Stark shift-related clock instability As shown in Figure 5, the Rb two-photon frequency standard operates with a fractional frequency instability of $3 \times 10^{-13}/\sqrt{\tau(s)}$ for τ from 1 s to 10,000 s.

V. CONCLUSIONS AND FUTURE OUTLOOK

We have demonstrated our system is capable of averaging down to 2.4×10^{-15} at 16,000 s. While we have only limited experimental data for timescales beyond this, we have seen that the clock instability increases on longer timescales. It appears that this performance degradation is related to the AC Stark shift, which would indicate that tighter control of the laser power is required to

achieve fractional frequency instabilities of 1×10^{-15} at one day. The initial optical design of the vapor cell assembly implemented a photodiode for use in laser power stabilization that was thermally anchored to temperature stage 2 for reduction of temperature influenced drifts. In some respects, the PMT used for fluorescence detection offers an improved measure of the average laser power across the atomic cloud because it relies on an atomic based signal rather than a beam sampling optic, for which the reflectivity is subject to polarization and temperature variations. Nevertheless, thermal considerations are still required, as the PMT's conversion efficiency is also temperature dependent [34]. Within the current design of the vapor cell assembly, an attempt was made to thermally connect the PMT to temperature stage 2, and fiberglass insulation was used to reduce thermal parasitics. However, temperature gradients are difficult to minimize over the 10 cm length of the PMT. Additionally, the PMT's high voltage power supply and transimpedance amplifier need to provide constant voltage and gain, respectively, in order to use the PMT as a long-term laser power sensor. Alternatively, if tighter control of laser power proves too challenging, there are several design modifications that allow the two-photon clock to operate with a smaller Stark shift. First, the spectral linewidth could be decreased by removing the helium contamination in the vapor cell; in our current cells, which are expected to be saturated with 4 mTorr of helium, the linewidth is approximately a factor of 2 larger than the natural linewidth. Removing the helium (through the use of a vacuum chamber or an helium-resistant cell [35]) would allow for a reduced laser power by a factor of 2 without affecting the short-term stability. Additional modifications include increasing the efficiency of the fluorescence detection; increasing the effective length of the vapor cell by routing the beam through the vapor on multiple non-overlapping passes; increasing the vapor density; and decreasing the desired short-term stability metric. Another final option is to increase the laser beam radius and laser power together; increasing both the power P and the intensity radius w_0 by a factor of F results in the same photon detection rate (accounting for both the decreased optical intensity and the increased number of atoms in the beam path) but a smaller overall AC Stark shift by the same factor F.

Beyond improvements to the stability, future work with this system necessarily involves miniaturizing and hardening the laser and frequency comb for future field deployment. Particular emphasis will need to be paid to automation of the locking electronics and simplification of the control loop architecture, which currently includes 10 independent temperature control segments. Reducing the power consumption of the frequency comb, which currently uses four pump lasers, is another important area of research. Finally, any attempt to prepare this type of advanced optical clock for space will have to overcome the challenge of radiation-induced darkening of optical components. Despite these challenges, we remain optimistic that a vapor cell optical clock, such as the one described here, could soon be deployed to provide precise timekeeping for a host of applications.

REFERENCES

[1] L. Maleki and J. Prestage, Metrologia **42**, S145 (2005).

[2] R. Wynands and S. Weyers, Metrologia **42**, S64 (2005).

[3] T. E. Parker, S. R. Jefferts, T. P. Heavner, and E. A. Donley, Metrologia **42**, 423 (2005).

[4] J. G. McNeff, IEEE Transactions on Microwave Theory and Techniques **50**, 645 (2002).

[5] V. Formichella, J. Camparo, and P. Travella, Applied Physics Letters (2017).

[6] D. J. Jones, S. A. Diddams, J. K. Ranka, A. Stentz, R. S. Windeler, J. L. Hall, and S. T. Cundiff, Science **288**, 635 (2000).

[7] S. A. Diddams, D. J. Jones, J. Ye, S. T. Cundiff, J. L. Hall, J. K. Ranka, R. S. Windeler, R. Holzwarth, T. Udem, and T. W. Hansch, Physical Review Letters **84**, 5102 (2000).

[8] R. Holzwarth, T. Udem, T. W. Hansch, J. C. Knight, W. J. Wadsworth, and P. S. J. Russell, Physical Review Letters **85**, 2264 (2000).

[9] N. Hinkley, J. A. Sherman, N. B. Phillips, M. Schioppo, N. D. Lemke, K. Beloy, M. Pizzocaro, C. W. Oates, and A. D. Ludlow, Science **341**, 1215 (2013).

[10] B. J. Bloom, T. L. Nicholson, J. R. Williams, S. L. Campbell, M. Bishof, X. Zhang, W. Zhang, S. L. Bromley, and J. Ye, Nature **506**, 71 (2014).

[11] T. Nicholson, S. Campbell, R. Hutson, G. Marti, B. Bloom, R. McNally, W. Zhang, M. Barrett, M. Safronova, G. Strouse, W. Tew, and J. Ye, **6**, 6896 (2015).

[12] N. Huntemann, C. Sanner, B. Lipphardt, C. Tamm, and E. Peik, Phys. Rev. Lett. **116**, 063001 (2016).

[13] C. W. Chou, D. B. Hume, J. C. J. Koelemeij, D. J. Wineland, and T. Rosenband, Physical Review Letters **104**, 070802 (2010).

[14] G. Grynberg and B. Cagnac, Reports on Progress in Physics **40**, 791 (1977).

[15] F. Nez, F. Biraben, R. Felder, and Y. Millerioux, Optics Communications **102**, 432 (1993).

[16] D. Touahri, O. Acef, A. Clairon, J.-J. Zondy, R. Felder, L. Hilico, B. de Beauvoir, F. Biraben, and F. Nez, Optics Communications **133**, 471 (1997).

[17] Hilico, L., Felder, R., Touahri, D., Acef, O., Clairon, A., and Biraben, F., Eur. Phys. J. AP **4**, 219 (1998).

[18] B. R. Washburn, S. A. Diddams, N. R. Newbury, J. W. Nicholson, M. F. Yan, and C. G. Jørgensen, Opt. Lett. **29**, 250 (2004).

[19] F. Adler, K. Moutzouris, A. Leitenstorfer, H. Schnatz, B. Lipphardt, G. Grosche, and F. Tauser, Opt. Express **12**, 5872 (2004).

[20] L. C. Sinclair, J.-D. Deschnes, L. Sonderhouse, W. C. Swann, I. H. Khader, E. Baumann, N. R. Newbury, and I. Coddington, Review of Scientific Instruments **86**, 081301 (2015), http://dx.doi.org/10.1063/1.4928163.

[21] A. Marian, M. C. Stowe, J. R. Lawall, D. Felinto, and J. Ye, Science **306**, 2063 (2004).

[22] J. Wu, D. Hou, Z. Qin, Z. Zhang, and J. Zhao, Phys. Rev. A **89**, 041402 (2014).

[23] K. D. Rathod and V. Natarajan, ArXiv e-prints (2015), arXiv:1511.05100 [physics.optics].

[24] N. D. Zameroski, G. D. Hager, C. J. Erickson, and J. H. Burke, Journal of Physics B: Atomic, Molecular and Optical Physics **47**, 225205 (2014).

[25] J. Snyder, Appl. Opt. (1975).

[26] E. Arimondo, M. Inguscio, and P. Violino, Reviews of Modern Physics **49** (1977).

[27] S. Bize, Y. Sortais, M. S. Santos, C. Mandache, A. Clairon, and C. Salomon, Europhysics Letters **45** (1999).

[28] G. C. Bjorklund, Opt. Lett. **5**, 15 (1980).

[29] L.-S. M. Jun Ye and J. L. Hall, Opt. Lett. **15**, 6 (1998).

[30] W. Zhang, M. J. Martin, C. Benko, J. L. Hall, J. Ye, C. Hagemann, T. Legero, U. Sterr, F. Riehle, G. D. Cole, and M. Aspelmeyer, Opt. Lett. **39**, 1980 (2014).

[31] W. M. Itano, L. L. Lewis, and D. J. Wineland, Phys. Rev. A **25**, 1233 (1982).

[32] J. W. Farley and W. H. Wing, Phys. Rev. A (1981).

[33] D. Tregubov, S. Snigirev, A. Golovizin, S. Pyatchenkov, D. Sukachev, A. Akimov, V. Sorokin, and N. Kolachevskyv, Journal of Physics : Conference Series **635** (2015).

[34] A. T. Young, Applied Optics **2**, 51 (1963).

[35] A. T. Dellis, V. Shah, E. A. Donley, S. Knappe, and J. Kitching, Opt. Lett. **41**, 2775 (2016).

DISTRIBUTION LIST

DTIC/OCP
8725 John J. Kingman Rd, Suite 0944
Ft Belvoir, VA 22060-6218   1 cy

AFRL/RVIL
Kirtland AFB, NM 87117-5776   1 cy

Official Record Copy
  AFRL/RVBN/Dr. Gretchen Phelps   1 cy

This page is intentionally left blank.